THE JOURNAL OF BIOLOGICAL CHEMISTRY VOL. 282, NO. 12, pp. 9090–9097, March 23, 2007

Site-specific Conformational Studies of Prion Protein (PrP) Amyloid Fibrils Revealed Two Cooperative Folding Domains within Amyloid Structure*[S]

Received for publication, September 6, 2006, and in revised form, January 16, 2007 Published, JBC Papers in Press, January 23, 2007, DOI 10.1074/jbc.M608623200

Ying Sun[‡], Leonid Breydo[‡1], Natallia Makarava[‡], Qingyuan Yang[‡2], Olga V. Bocharova[‡3], and Ilia V. Baskakov[‡§4]

From the [‡]Medical Biotechnology Center, University of Maryland Biotechnology Institute, Baltimore, Maryland 21201 and the [§]Department of Biochemistry and Molecular Biology, University of Maryland, Baltimore, Maryland 21201

Despite the ability of most proteins to form amyloid, very little is know about amyloid fibril structures and the factors that govern their stability. Using amyloid fibrils produced from full-length prion protein (PrP), we describe a reliable approach for determining both site-specific and global conformational stability of the fibrillar form. To measure site-specific stability, we produced six variants of PrP by replacing the residues at positions 88, 98, 127, 144, 196, and 230 with cysteine, labeled the new cysteines with the fluorescent dye acrylodan, and investigated their conformational status within the amyloid form in guanidine hydrochloride-induced denaturation experiments. We found that the fibrils labeled at positions 127, 144, 196, and 230 displayed cooperative unfolding and showed a very high $C_{1/2}$ value similar to that observed for the global unfolding of the amyloid structure. The unfolding at residue 98 was also cooperative; however, it showed a $C_{1/2}$ value substantially lower than that of global unfolding, whereas the unfolding of fibrils labeled at residue 88 was non-cooperative. These data illustrate that there are at least two independent cooperative folding domains within the amyloid structure of the full-length PrP. In addition, kinetic experiments revealed only a partial overlap between the region that constituted the fibrillar cross-β core and the regions that were involved in nucleation. This result illustrates that separate PrP regions accounted for the nucleation and for the formation of the conformationally most stable fibrillar core.

Besides the native globular shape, the vast majority of proteins and peptides are capable of forming alternative, well defined structures with a specific cross-β sheet fold referred to as amyloid fibrils (1). In contrast to native folds, however, amyloid fibrils display high conformational stability and unusual mechanical properties. Because of their peculiar properties, amyloid structures have been exploited in nature for a variety of physiological functions. For example, the major structural component of the shells of many insects and fish is made of amyloid that protects developing embryos from mechanical pressure, dehydration, and proteolytic digestion (2, 3). Another example of naturally occurring amyloid includes the extracellular curly fibrils produced by *Escherichia coli* that enable the bacteria to colonize a surface (4). Mammalian cells utilize amyloid structures made of Pmel17 protein for the biogenesis of melanin (5). These findings illustrate that that amyloid formation is an evolutionarily preserved biological pathway used to produce natural biomaterials with extraordinary physical properties and important physiological functions.

For the same reasons that amyloid fibrils are exploited in nature to fulfill certain functions, they could be detrimental to human health. Because of their high conformational and kinetic stability, fibrillar deposits can accumulate inside or outside of cells and initiate pathological processes leading to neurodegenerative or systemic diseases (6, 7). High resistance to temperature or solvent-induced denaturation and to proteolytic digestion enables fibrils of the prion protein to transmit prion diseases (8, 9) or fibrils of yeast prion proteins to act as a heritable determinant of phenotype (10). Remarkably, different isolates or strains of the disease-specific fibrillar form of PrP[5] (PrP^{Sc}) exhibit substantial differences in conformational stability, an important physical property that appears to be tightly linked to neuropathological features and incubation time of prion disease (11–15). Interspecies transmission of prions was found accompanied by a change in conformational stability and disease phenotype, leading to the emergence of new prion strain (12). Recent studies of yeast prion protein Sup35 reveal a strong link between conformational stability and the intrinsic infectivity of fibrils generated *in vitro* (16).

Regardless of whether amyloid structures are involved in normal function or associated with pathological processes, the physical properties of fibrils such as conformational stability appear to determine to a large extent their biological effects. In

* This work was supported by the Prion Program at the University of Maryland Biotechnology Institute. The costs of publication of this article were defrayed in part by the payment of page charges. This article must therefore be hereby marked "*advertisement*" in accordance with 18 U.S.C. Section 1734 solely to indicate this fact.

[S] The on-line version of this article (available at http://www.jbc.org) contains three supplemental figures.

[1] Present address: Dept. of Molecular Biology and Biochemistry, University of California, Irvine, CA 92697.

[2] Present address: Dept. of Pharmacology and Experimental Therapeutics, University of Maryland, Baltimore, MD, 21201.

[3] Present address: Institute of Bioorganic Chemistry, Russian Academy of Sciences, Moscow, Russia, 117997.

[4] To whom correspondence should be addressed: Medical Biotechnology Center, University of Maryland Biotechnology Institute, 725 W. Lombard St., Baltimore, MD 21201. Tel.: 410-706-4562; Fax: 410-706-8184; E-mail: Baskakov@umbi.umd.edu.

[5] The abbreviations used are: PrP, full-length recombinant prion protein; PrP^{C}, cellular isoform of the prion protein; PrP^{Sc}, disease associated isoform of the prion protein; WT, wild type; PK, proteinase K; GdnHCl, guanidine hydrochloride; HPLC, high pressure liquid chromatography; MES, 4-morpholineethanesulfonic acid; ThT, thioflavin T; FTIR, fourier transform infrared.

contrast to the native state, surprisingly little is known about physical properties of amyloid structures or factors that determine their conformational stability. Because individual polypeptides are able to form conformationally different fibrils, both amino acid sequence and folding conditions should impact the final fibrillar structure (17). Lack of well developed physical approaches together with insolubility and heterogeneity of amyloid fibrils have imposed substantial difficulties in elucidating their conformational properties.

In the present study, we have described a reliable approach for elucidating the global and site-specific conformational stability of amyloid fibrils. We employed this method to elucidate the conformation of fibrils produced from the full-length mouse PrP. Our approach consists of several steps including (i) generating individual Cys-PrP variants; (ii) labeling of individual Cys-PrP variants with the fluorescent probe acrylodan; (iii) conversion of Cys-PrP variants into amyloid fibrils; and (iv) measuring GdnHCl-induced denaturation using acrylodan fluorescence. We found that within the amyloid fibrillar structure, PrP polypeptides adopt two independent folding domains. These domains are characterized by different $C_{½}$ values in GdnHCl-induced denaturation. The denaturation profile of the most stable domain was superimposable with the global unfolding of amyloid structure. This domain appears to form cross-β-sheet fibrillar core, whereas the less stable domain might be responsible for forming interfaces between filaments. The kinetics of fibril formation revealed that residues 88, 98, 196, and 230 play more prominent roles in nucleation than residues 127 or 144. Our studies established a new technique for studying amyloid fibrils and provided an important new insight into the substructure of PrP fibrils.

EXPERIMENTAL PROCEDURES

Expression and Purification of Cys-PrP Variants—W88C, W98C, Y127C, W144C, N196C, and S230C point mutations were introduced into the mouse *PrP23–230* gene using the QuikChange procedure, and the results were verified by sequencing. WT and Cys-PrP variants DNA in pET101/D-TOPO vector (Invitrogen) were transfected into BL21(DE3) Star cells (Invitrogen).

Cys-PrP variants were expressed and purified as described previously (18, 19) with the following modifications. After gel filtration, the fractions containing PrP (~0.3 mg/ml in 6 M urea, 100 mM Tris-HCl, pH 7.5) were supplemented with EGTA and L-cystine (to final concentrations of 5 and 0.2 mM, respectively), incubated at 23 °C for 1 h, and dialyzed against 3 M urea, 100 mM Tris-HCl, 5 mM EGTA, 0.2 mM L-cystine, pH 7.5, overnight to achieve formation of a native disulfide bond. All subsequent steps were as described previously (18, 19). The purified Cys-PrP variants were confirmed by SDS-PAGE (supplemental Fig. 1*a*) and electrospray mass spectrometry to be a single species with an intact disulfide bond and correct molecular weight.

Labeling of PrP with Acrylodan—A typical labeling reaction consisted of mixing the Cys-PrP variant (1 mg/ml, 42 μM, 300 μl) with ammonium acetate (1 M, pH 7.0, 3 μl), Tris(2-carboxyethyl)phosphine (5 mM in water, 5 μl, 2 eq), and acrylodan (50 mM in Me_2SO, 5 μl, 25 eq) and then incubation for 2 h at 23 °C, addition of Tris(2-carboxyethyl)phosphine (5 mM, 2.5 μl), and incubation for another 4 h. The reaction mixture was then centrifuged at 10,000 rpm for 8 min, and the supernatant was purified by HPLC (Symmetry 300 C4, 4.6×250 mm; Waters Corp.; eluant gradient consisted of 1 → 60% acetonitrile in water containing 0.1% trifluoroacetic acid) at a flow rate of 0.8 ml/min. The typical yield of product was ~180 μg (60%). The identity and purity of the acrylodan-labeled protein was verified by electrospray ionization-mass spectrometry and SDS-PAGE, and the native conformation was confirmed by CD (supplemental Fig. 1*b*).

Conversion of PrP into Amyloid Fibrils and Measurement of the Kinetics of Fibrilization—To form amyloid fibrils, the stock solution of WT PrP (3 mg/ml in 6 M GdnHCl) was mixed with a solution of freshly prepared acrylodan-labeled Cys-PrP variant at a molar ratio of 9:1 and diluted to a final total protein concentration of 0.25 mg/ml in 50 mM MES buffer, 2 M GdnHCl, pH 6.0. The reaction mixture was incubated at 37 °C in with continuous shaking at 600 rpm as described previously (19). The kinetics of fibril formation was monitored simultaneously using acrylodan florescence and ThT binding assays. Aliquots withdrawn during the time course of incubation at 37 °C were diluted with 5 mM sodium acetate buffer (pH 5.5) to a final PrP concentration of 0.3 μM. For monitoring acrylodan fluorescence, two emission spectra (from 380 to 600 nm) were recorded for each sample in 0.4-cm rectangular cuvettes with an excitation at 370 nm using a Flurmax-3 fluorometer (Jobin Yvon) with both excitation and emission slits 3 nm and averaged. Then ThT was added to the same sample to a final concentration of 10 μM, and ThT florescence was measured as previous described. FTIR spectroscopy and electron microscopy of amyloid fibrils were performed as described previously (18).

Determining Site-specific Conformational Stability—To determine the site-specific conformational stability, the fibrils produced from mixtures of WT and acrylodan-labeled Cys-PrP variants were diluted to a final PrP concentration of 6.9 μg/ml (equivalent of 0.3 μM) and incubated for 1 h in solutions containing different concentrations of GdnHCl (from 0 to 7 M GdnHCl, in 0.1 M MES buffer, pH 6.0) at 23 °C. The acrylodan emission spectra were recorded as described earlier.

Determining Global Stability—The fibrils produced from mixtures of WT and acrylodan-labeled Cys-PrP (7 μl, 0.25 mg/ml) were suspended in MES (30 μl, 100 mM, pH 6.0) containing different concentrations of GdnHCl. The solution was incubated for 1 h at 23 °C and then diluted to 300 μl with 9 M GdnHCl and water to adjust the final concentration of GdnHCl to 0.55 M. Fluorescence spectra were recorded in the presence of 10 μM ThT as previous described.

RESULTS

Generating Cys Variants of PrP—To determine the specific positions for Cys substitutions, we used several criteria. First, we avoided replacing the residues that are known to be "functionally" important for PrP^{Sc} propagation, such as the residues involved in the dominant-negative effect (20), the residues that account for the species-species barrier, or those associated with familial forms of prion disease (21). Second, because we wanted to minimize the possible perturbation effects of the acrylodan-

labeled Cys on fibrillar conformation, we replaced the bulky amino acid residues, such as tryptophans at positions 88, 98, or 144, tyrosine at 127, or asparagine at 196. We also replaced serine at position 230. Because in PrP^C glycans and the glycosylphosphatidylinositol anchor are attached to asparagine 196 and serine 230, respectively, we assumed that labeling PrP at these residues should have minimal steric impact on fibril formation. To date, we have produced six PrP variants: W88C, W98C, Y127C, W144C, N196C, and S230C.

All six Cys variants were expressed and purified to homogeneity using the protocols developed for WT PrP (19, 22), with some minor modifications as specified under "Experimental Procedures" (supplemental Fig. 1*a*). We took special precaution with respect to the formation of the proper disulfide bonds in Cys-PrP variants by performing oxidative refolding in partially denaturing conditions (3 M urea; 100 mM Tris-HCl, 5 mM EGTA, 0.2 mM L-cystine, pH 7.5, overnight incubation). In the presence of 3 M urea, the native α-helical conformation is still stable and favors formation of the proper disulfide bridge while precluding formation of the non-native disulfide bridges. The oxidative refolding was followed by a reverse-phase HPLC, by which correctly folded α-helical PrP monomers were separated from incorrectly folded PrP species including those with non-native disulfide bonds.

All six Cys-PrP variants were labeled with acrylodan; the reaction mixture was purified again by HPLC to separate labeled and unlabeled PrP molecules ("Experimental Procedures") (supplemental Fig. 1*b*). Acrylodan offers several advantages as a fluorescence probe such as high photostability, high sensitivity to the solvent environment, and a relatively low molecular weight (similar to that of tryptophan). This dye has been used successfully for studying conformational properties of amyloid fibrils produced from the yeast prion Sup35 (23).

Converting Cys Variants into Fibrillar Form—To form amyloid fibrils from the Cys-PrP variants, we use the protocol previously developed in our laboratory (shaking at 2 M GdnHCl, pH 6.0) (19, 24). In producing fibrils, it was important to make sure that the Cys substitutions and subsequent labeling with acrylodan did not alter the conformational properties of the fibrillar form. To minimize a possible perturbation effect, we used 9:1 molar mixtures of WT PrP and acrylodan-labeled Cys-PrP variants for the conversion reactions. To test whether acrylodan-labeled Cys-PrP affected physical properties of fibrils, we employed a proteinase K digestion assay for assessing the PK-resistant core, FTIR spectroscopy for evaluating possible perturbations in secondary structure, and electron microscopy for confirming fibrillar morphology. The PK digestion assay showed that the fibrils produced from the mixtures of six different Cys-PrP variants and WT PrP had a PK-resistant core identical to that of WT fibrils (supplemental Fig. 2). FTIR spectroscopy revealed identical secondary structure in WT PrP fibrils and in fibrils produced from the mixtures of WT and Cys-PrP variants (supplemental Fig. 3). The second derivatives of FTIR spectra showed two major peaks at 1616 and 1626 cm^{-1} that correspond to β-sheets in all samples and a peak at 1662 cm^{-1} that corresponds to β-turns and loops. Electron microscopy confirmed that high-order well defined fibrils consisting of several laterally assembled filaments were formed in the mixtures of WT and Cys variants (Fig. 1). These fibrils were morphologically similar to those produced from WT PrP (25). Taken together, these data confirmed that the incorporation of acrylodan-labeled Cys-PrPs into fibrils did not have noticeable effects on fibrillar secondary structure, the size of the PK-resistant core, or the ability of filaments to assemble into mature high-order fibrils.

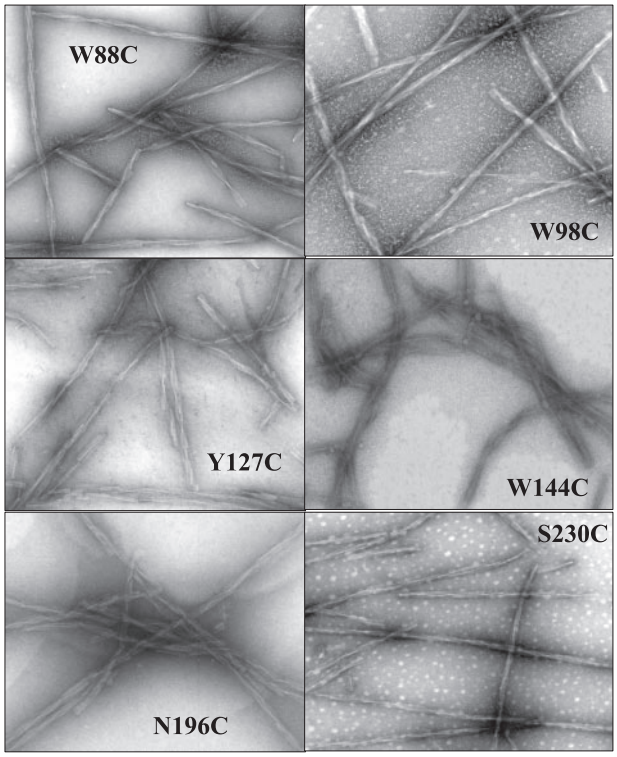

FIGURE 1. **Electron microscopy of amyloid fibrils produced from the mixtures of WT and Cys-PrP variants.** WT and six Cys-PrP variants labeled with acrylodan were mixed at a molar ratio of 9:1 and incubated under standard reaction conditions as described under "Experimental Procedures." Negative staining and electron microscopy were performed as described previously (18).

Determining the Site-specific Conformational Stability—To determine the site-specific conformational stability, the fibrils produced from mixtures of acrylodan-labeled Cys-PrP variants and WT PrP were incubated in solutions containing increasing concentrations of GdnHCl (from 0 to 7 M, in 0.1 M MES buffer, pH 6.0, for 1 h, at 23 °C) followed by measurement of steady-state acrylodan fluorescence. Our preliminary studied revealed that the incubation of fibrils for 1 h was enough to reach apparent equilibrium. With an increase in GdnHCl concentration, the acrylodan emission spectra displayed a decrease in fluorescence intensity and a red shift in λ_{max} (Fig. 2*a*). Because acrylodan is highly sensitive to solvent polarity within its immediate environment, its emission maximum shifts from 460 to 470 nm in a non-polar environment such as the protein interior to ~520 nm in a polar environment such as water. The red shift in λ_{max} was consistent with removal of acrylodan-labeled residues from the fibrillar interior into the solvent environment. Therefore, for probing the conformational status of different PrP regions in GdnHCl-induced denaturation, we used λ_{max} of acrylodan emission as an observable parameter.

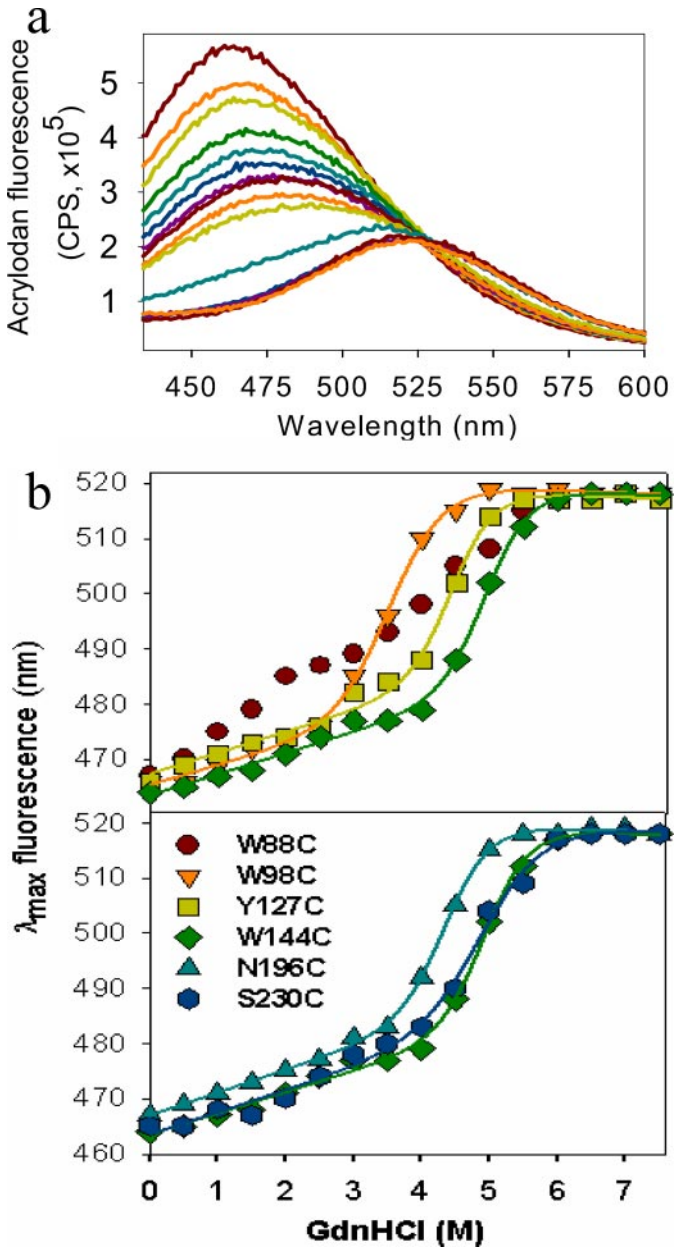

FIGURE 2. **GdnHCl-induced denaturation of the amyloid fibrils.** *a*, acrylodan emission spectra monitored at different concentrations of GdnHCl (from 0 to 7 M) for the fibrils produced from a mixture of WT and PrP W144C variant labeled with acrylodan. Upon denaturation, the emission spectra showed a decrease in the fluorescence intensity and a red shift in λ_{max}. *b*, GdnHCl-induced denaturation profiles recorded for the fibrils produced from mixtures of WT PrP and the following acrylodan-labeled PrP variants: W88C (●), W98C (▼), Y127C (■), W144C (◆), N196C (▲), and S230C (●). The *solid curves* represent the fits of the data to a two state model of protein unfolding (31).

The site-specific denaturation profiles for fibrils labeled at residues 98, 127, 144, 196, and 230 showed cooperative, apparent two-state transitions, whereas the unfolding profile for fibrils labeled at residue 88 displayed a non-cooperative transition (Fig. 2*b*). The non-cooperative unfolding at residue 88 correlated well with the high susceptibility of the N-terminal region to PK digestion in recombinant fibrils and in PrP^{Sc} (22, 26, 27). This region is not essential for prion infectivity and is outside of the structured PrP^{Sc} domains (28, 29).

TABLE 1

Thermodynamic parameters for GdnHCl-induced unfolding of PrP amyloid fibrils

The thermodynamic parameters are results of nonlinear, least-squares best fits of the data using a linear extrapolation method (31).

Fibrils were produced from	$\Delta G°$	m	$C_{½}$	$C_{½}$ [a]
	kcal/mol	*kcal/mol* × M	M	M
WT & W88C				4.77
WT & W98C	−5.36 ± 0.53	1.50 ± 0.14	3.57	4.83
WT & Y127C	−8.52 ± 0.93	1.90 ± 0.20	4.47	4.82
WT & W144C	−9.07 ± 0.90	1.82 ± 0.18	4.97	4.84
WT & N196C	−7.87 ± 0.43	1.79 ± 0.10	4.40	4.85
WT & S230C	−6.47 ± 0.76	1.30 ± 0.20	4.98	4.92
WT				4.95

[a] These $C_{½}$ values were determined from ThT-assay and represent global unfolding of amyloid structure.

To calculate the thermodynamic parameters for the residues that exhibited cooperative unfolding, we used non-linear fitting of the denaturation profiles to the two-state model of protein unfolding (30, 31). The Gibbs free energy $\Delta G°$, the cooperativity of unfolding (the m values), and the $C_{½}$ values calculated from this fitting are presented in Table 1. Both $\Delta G°$ and the $C_{½}$ values are typically used for evaluating the conformational stability of globular proteins. However, because $\Delta G°$ is estimated from the linear extrapolation of ΔG from the transition zone to zero concentration of the denaturant, a functional dependence that could be non-linear (30, 32), the $C_{½}$ value may provide a more direct measure of the conformational stability than $\Delta G°$.

The $C_{½}$ values for residues 127, 144, 196, and 230 were all found to be within a relatively narrow range (between 4.47 and 4.98 M of GdnHCl, Table 1), suggesting that these residues are likely to belong to the same structural domain. Surprisingly, the site-specific stability for residue 98 was substantially lower ($C_{½}$ = 3.57 M) than those determined for the aforementioned residues (Table 1, Fig. 2*b*). These data suggest that at least two independent structural domains were formed within amyloid fibrils. Both domains exhibited cooperative unfolding; however, they displayed markedly different conformational stabilities. Indeed, at 4 M GdnHCl, the domain associated with residue 98 was largely unfolded, whereas the domain encompassed by residues 127 and 230 was still folded.

The Site-specific Denaturation at Residues 144 and 230 Coincides with the Global Unfolding of Amyloid Structure—Although our studies defined the site-specific denaturation profiles for selected residues, it is not known whether any of the site-specific denaturation curves represented global unfolding of amyloid cross-β-structure. To address this question, we measured the GdnHCl-induced denaturation profiles using a ThT binding assay. Because ThT selectively binds to amyloid structures, this assay offers a rapid and sensitive way for quantitative measurement of the amount of amyloid structure, therefore offering a tool for monitoring the global unfolding of fibrils. As determined from the ThT assay, the $C_{½}$ values for global unfolding were nearly identical (ranging between 4.77 and 4.95 M), regardless of whether the fibrils were formed solely from WT or from mixtures of WT and acrylodan-labeled Cys-PrP variants (Fig. 3 and Table 1). The denaturation profiles measured by the ThT assay were superimposable for all six mixtures with that of WT (Fig. 3). These experiments demonstrated that (i) incorporation of the acrylodan-labeled Cys-PrP

variants into fibrils did not alter the global stability of fibrils and (ii) the conformational stability determined for residues 144 and 230 represents the global stability of amyloid structure as judged from the $C_{1/2}$ values. The site-specific stabilities at positions 127 and 196 were slightly lower than those for residues 144 and 230 ($C_{1/2}$ = 4.47 and 4.40 M *versus* 4.97 and 4.98 M, respectively). It is likely that residue 127 is at the edge of the region that constitutes the fibrillar core, whereas residue 196 might be in the vicinity of the fibrillar interface. Taken together, our results indicate that the region ~127–230 appears to adopt conformationally the most stable cross β-sheet core in the amyloid fibrils. Next we were interested in knowing whether the PrP region that adopts cross β-sheet core was also responsible for the initial interactions during nucleation stage of fibrilization.

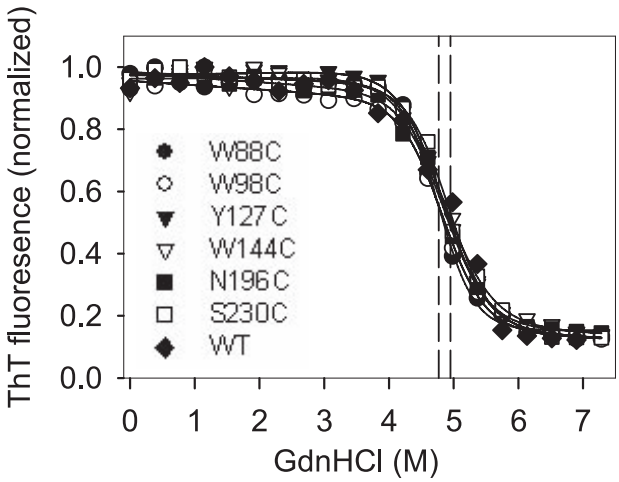

FIGURE 3. **Global denaturation of amyloid fibrils analyzed by ThT fluorescence assay.** GdnHCl-induced denaturation profiles were monitored for fibrils produced from mixtures of WT PrP and the following acrylodan-labeled PrP variants: W88C (●), W98C (○), Y127C (▼), W144C (▽), N196C (■), S230C (□), or WT PrP (◆) using a ThT fluorescence assay. The *solid curves* represent the fits of the data to a two-state model of protein unfolding (31). The *dashed lines* define the variation range for the $C_{1/2}$ values (from 4.77 to 4.95 M), which were derived from the curve fittings.

The N-terminal and C-terminal Regions Are Involved in Nucleation—To identify the sites that were involved in the nucleation, we monitored the kinetics of amyloid formation in parallel using two assays, ThT binding and acrylodan fluorescence. Although the ThT binding assay reports formation of amyloid structures, the acrylodan fluorescence monitors the local environment of the residues labeled with this dye. Therefore, the acrylodan fluorescence assay determines whether specific residues are exposed to the solvent or buried in the protein interior as a function of polymerization time.

The lag phases and kinetic profiles of acrylodan fluorescence was very similar for all six mixtures of WT and acrylodan-labeled Cys-PrP variants (Fig. 4 and Table 2). This indicates that the acrylodan probe becomes shielded from the aqueous solvent at similar rates regardless of the site-specific position of the label. As judged from the ThT assay, however, the reaction mixtures containing any one of four acrylodan-labeled Cys-PrP variants (88, 98, 196, and 230) displayed substantially longer lag phase (~1.5–2-fold) than the mixtures with the variants 127 or 144 or for WT PrP alone (Fig. 4 and Table 2). The kinetics of polymerization in the mixtures of WT and variants 127 or 144 were similar to that observed for WT PrP alone (Fig. 4 and Table 2). Therefore, although the residues at all six positions were secluded at the same rate, the modification at four residues (88, 98, 196, and 230) prolonged the lag phase for forming mature fibrils presumably via interfering with specific intermolecular associations occurring at the early stages of polymerization. In other words, PrP variants (88, 98, 196, and 230) showed an increase in acrylodan fluorescence much earlier than ThT fluorescence (Fig. 4 *a*, *b*, *e*, and *f*, and Table 2), whereas the variants 127 and 144 displayed a simultaneous increase in acrylodan and ThT fluorescence (Fig. 4, *c* and *d*). These experiments illustrate that residues 88, 98, 196, and 230 were excluded from the solvent prior to the formation of the amyloid structure, whereas residues 127 and 144 were displaced from the solvent environment into the protein interior simultaneously with the acquisition of a fibrillar structure. Taken

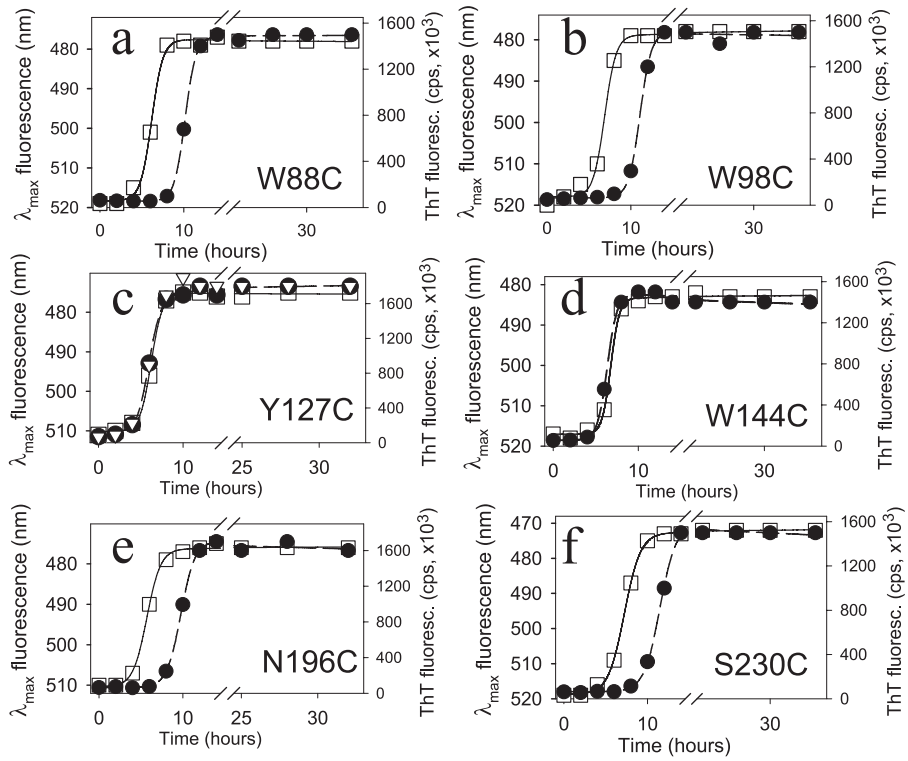

FIGURE 4. **Kinetics of amyloid fibril formation.** The kinetics of fibril formation was monitored in reaction mixtures of WT PrP and the following acrylodan-labeled PrP variants: W88C (*a*), W98C (*b*), Y127C (*c*), W144C (*d*), N196C (*e*), or S230C (*f*) using an acrylodan fluorescence assay (□) and a ThT fluorescence assay (●). 9:1 molar mixtures of WT PrP and acrylodan-labeled Cys-PrP variants were used in standard reaction conditions as described under "Experimental Procedures." The kinetics of fibril formation from WT PrP using the ThT assay is shown on *panel c* (▽).

TABLE 2

The lag phase of PrP amyloid formation as determined from ThT and acrylodan fluorescence assays

The length of the lag-phase were calculated by fitting the kinetic curves as previously described (24).

Fibrils were produced from	Lag phase[a]	Lag phase[b]
	h	*h*
WT and W88C	9.18 ± 0.3	4.8 ± 0.2
WT and W98C	9.7 ± 0.3	5.5 ± 0.2
WT and Y127C	4.7 ± 0.2	4.9 ± 0.2
WT and W144C	5.4 ± 0.2	5.7 ± 0.2
WT and N196C	8.1 ± 0.3	4.1 ± 0.2
WT and S230C	9.6 ± 0.3	5.3 ± 0.2
WT	4.7 ± 0.2	

[a] The lag phase was determined from ThT fluorescence assay.
[b] The lag phase was determined from acrylodan fluorescence assay.

together, these data indicate that residues 88, 98, 196, and 230 play more prominent roles in nucleation.

DISCUSSION

The past 40 years of protein folding studies revealed fundamental rules that describe how proteins adopt their native conformation. Beside a native globular shape, the vast majority of proteins and peptides are capable of forming alternative structures called amyloid fibrils (1). Despite the fact that the ability to acquire amyloid structure appears to be generic (1), fibrilization of a relatively small number of polypeptides was found to be pathogenic and linked to several neurodegenerative and systemic diseases (6, 7). Among amyloidogenic proteins, even fewer were shown to be able to form fibrils with the peculiar property of transmitting a disease or acting as a heritable determinant of phenotype (8, 10). Those are the mammalian and yeast prion proteins, respectively. Why are some but not all amyloidogenic proteins capable of forming infectious fibrils? Why are some but not all types of amyloid fibrils made of the same proteins infectious? Defining infectious *versus* non-infectious amyloid structures is one of the most intriguing questions in biomedical research (15).

Recent studies of the yeast prion protein Sup35 reveal a strong link between conformational stability and infectivity of amyloid fibrils generated *in vitro* (16). The fibrils that displayed low conformational stability were found to exhibit a high efficiency of infection, with the large majority of resulting yeast colonies showing a strong phenotype ("strong" strains) (16). Conversely, fibrils with high conformational stability displayed low infectivity and produced "weak" strains. In yeast prions, weak strains are defined as those that disappear quickly or are easily cured, whereas strong strains are characterized by their ability to sustain fast growing colonies for a long period of time. The question of whether the same rule applies to mammalian prion fibrils is of great interest.

Although several robust methods have been developed in the past for measuring the conformational stability of natively folded, globular proteins, the stability of amyloid fibrils is difficult to assess due to their highly aggregated, heterogeneous, and sometimes insoluble nature. In recent studies, Wetzel and co-authors (33, 34) described an elegant method where the conformational stability of the Aβ fibrils was evaluated via measurement of the final monomer concentration after the process of fibril elongation reached an equilibrium. This method was successful in evaluating the effect of single-point mutations on the global stability of fibrils (34); however, it can be employed only if 100% of polypeptides are amyloidogenic and no alternative aggregation pathways take place beside amyloid formation.

In the present study, we described an alternative technique for probing the conformational stability of amyloid fibrils. To assess stability, we applied the same formal approach that was originally developed for evaluating the stability of globular proteins, in which the thermodynamic parameters such as ΔG°, m, and $C_{1/2}$ are derived from the linear extrapolation of the transition curves to zero concentration of denaturant. We have illustrated that this method could be employed for measuring the global stability and for assessing the conformational status of different regions within the complex amyloid structure.

The global conformational stability of PrP fibrils determined in our studies was compatible with those reported for fibrils generated *in vitro* from other amyloidogenic polypeptides. Goto and co-authors (35) reported $\Delta G^\circ = -10.5$ kcal/mol for fibrils prepared from β2-microglobulin. The fibril elongation approach revealed ΔG° of -9 kcal/mol for Aβ fibrils (33). These ΔG° values are substantially higher than ΔG° of natively folded globular proteins, arguing that the amyloid structure is the most stable protein conformation. The observations that many proteins are able to adopt alternative amyloid structures and that the amyloid state is conformationally more stable than the native state require us to revisit the basic rules of protein folding such as the position of the native state in the energy landscape. An alternative view proposes that most polypeptides including PrP are trapped for their entire protein lifetime in a native state that does not correspond to a free energy minimum, whereas global energy minima are occupied by amyloid structures, which are kinetically inaccessible under physiological conditions.

Using newly developed techniques, we probed the conformational status of six PrP regions within the amyloid form. In evaluating ΔG°, it is necessary to extrapolate the posttransition baseline toward zero concentration of denaturant. Although linear extrapolations have been typically used to derive ΔG°, recent studies of several globular proteins including PrP revealed that the denatured ensembles often display thermodynamically variable behavior, bringing the validity of the linear extrapolation method into question (30, 36, 37). Therefore, the $C_{1/2}$ value may provide a more direct way to evaluate the conformational stability than ΔG°. As judged from the $C_{1/2}$ values, the site-specific conformational stability of the residues within the region 127–230 were found to be similar to the global stability of the amyloid structure, whereas the stability of residue 98 was substantially lower than the global stability but approached that of natively folded proteins (Table 1). In a simplistic view, the amyloid fibrils consist of a cross-β-core core and structural motifs that form the fibrillar interface and participate in lateral interaction between filaments within mature fibrils. Based on $C_{1/2}$ values, residues 127, 144, 196, and 230 should be involved in forming the cross-β-core, which would account for the high conformational stability and structural

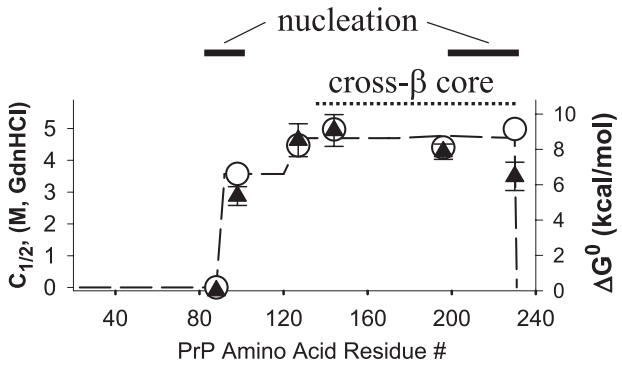

FIGURE 5. **The site-specific $\Delta G°$ (▲) and $C_{1/2}$ (○) of PrP amyloid fibrils.** The *dashed line* shows the conformational stability profile, as judged from the $C_{1/2}$. The denaturation at residue 88 was non-cooperative; therefore, its $C_{1/2}$ was assumed to be 0 M GdnHCl. The region that constitutes the conformationally most stable cross-β core is marked by the *dotted line*, whereas the regions that are involved in nucleation are marked by *bold solid lines*.

integrity of fibrils, whereas residue 98 is likely to be a part of the filament interface (Fig. 5).

The *m* value represents the cooperativity of protein unfolding and is generally thought to be proportional to the amount of newly accessible surface area exposed upon denaturation. The basis of this claim is largely derived from the theoretical work of Schelman (39), as well as from correlations observed between the *m* values and accessible surface area (38). Notably, although the *m* values for residues 127, 144, and 196 were found to be similar to each other, residue 230 displayed a substantially lower *m* value despite the fact that all four residues showed similar $C_{½}$ and appear to be involved in forming the fibrillar core (Table 1). In reconciling these differences, it is important to acknowledge that the *m* value can reflect molecular properties additional to the changes in surface area on denaturation. Cara and Privalov (40) showed that the presence of unfolding intermediate states will lower the *m* values of solvent-induced denaturation. The extent to which each specific region undergoes subglobal or local unfolding may impose an additional impact on *m* values (41). Because site-specific denaturation profiles reflect both global and local unfolding, it is likely that the differences in *m* values arise due to differences in local unfolding of different PrP regions within the amyloid fibrillar core. Because residue 230 is at the last C-terminal position, the denaturation profile for this residue appears to be affected to a large extent by local unfolding.

The data on site-specific conformational stability presented in the current studies were in good agreement with our former studies. We have previously shown that the C-terminal part of PrP encompassing residues 138–230 was the most resistant to proteinase K digestion in the amyloid form (22, 26). Furthermore, the epitopes within this C-terminal region were found to be buried and resistant to GdnHCl-induced denaturation, whereas the epitope to antibody D13 (residues 95–105) was shown to be solvent-accessible (42).

Taken together, all three approaches argue that residues 138–230 and, possibly, 127–230 are solvent-protected and adopt cross-β-sheet core in the fibrillar form. Because this region accounts for high conformational stability of fibrils, we were interested in knowing whether the same part of the PrP molecule was involved in intermolecular associations at the early stages of polymerization referred to as nucleation. The nucleation event occurs prior to formation of mature amyloid structure. Therefore, we used acrylodan fluorescence to determine whether the residues labeled with acrylodan were secluded from the solvent at the same time or prior to the formation of amyloid structure. Our data demonstrate that the N-terminal (residues 88 and 98) and the C-terminal (residues 196 and 230) regions were sequestered from the solvent prior to formation of the mature amyloid structure, indicating that these four residues play more prominent roles in nucleation than other two residues (Fig. 5). Whether PrP molecules interact in a "head-to-head" or "head-to-tail" fashion remains to be determined in future studies. Nevertheless, these results were consistent with the former work, where the N-terminal region including octarepeats was shown to be involved in polymerization of PrP *in vitro* or in development of prion disease *in vivo* (28, 43–45). Transgenic mice that expressed truncated PrP 90–230 lacking octarepeats were shown to develop scrapie infection with a much longer incubation time than wild-type mice (28). Similarly, our former studies revealed that truncated PrP 90–230 polymerizes slower than full-length PrP (43). Furthermore, insertion of additional octarepeats were shown to increase the rate of polymerization of PrP peptides (44) or the efficacy of the interaction between PrP^C and PrP^{Sc} (45). Therefore, although not essential for infectivity, the N-terminal region definitely influences the rate of intermolecular interaction during prion replication.

The plausible involvement of the C-terminal region in nucleation revealed in this work was in good agreement with former studies. A simulation by Dima and Thirumalai (46) suggests that residues 172–224, which correspond to helices B and C in the native PrP^C form, have a high propensity to adopt a β-sheet rich conformation in the PrP^* form, a possible intermediate on the way to the fibrillar form. Furthermore, crystallographic studies of the α-helical PrP monomer suggested that the region 188–204 is able to undergo a partial α-helix- to β-sheet-switch within the monomeric state, presumably giving rise to early intermediate species (47). Noteworthy, a bulky non-polar substitution at position 230, a mimic of a glycosylphosphatidylinositol anchor, substantially delayed the nucleation and partially impaired amyloid fibril formation (48). Our results were also consistent with the remarkably high intrinsic helix propensity of residues within the helix A (residues 144–154), which are highly stable to denaturing conditions and, therefore, less likely to initiate transition into the fibrillar form (49).

Acknowledgment—We thank Pamela Wright for editing the manuscript.

REFERENCES

1. Dobson, C. M. (2002) *Trends Biochem. Sci.* **24,** 329–332
2. Iconomidou, V. A., Vriend, G., and Hamodrakas, K. (2000) *FEBS Lett.* **479,** 141–145
3. Podrabsky, J. E., Carpenter, J. E., and Hand, S. C. (2001) *Am. J. Physiol.* **280,** R123–R131
4. Chapman, M. R., Robinson, L. S., Pinkner, J. S., Roth, R., Heuser, J., Hammar, M., Normark, S., and Hultgren, S. J. (2002) *Science* **295,** 851–855
5. Fowler, D. M., Koulov, A. V., Alory-Jost, C., Marks, M. S., Balch, W. E., and

Kelly, J. W. (2006) *PLoS Biol.* **4,** 100–107
6. Carrell, R. W., and Lomas, D. A. (1997) *Lancet* **350,** 134–138
7. Prusiner, S. B. (2001) *N. Engl. J. Med.* **344,** 1516–1526
8. Legname, G., Baskakov, I. V., Nguyen, H.-O. B., Riesner, D., Cohen, F. E., DeArmond, S. J., and Prusiner, S. B. (2004) *Science* **305,** 673–676
9. Castilla, J., Saa, P., Hetz, C., and Soto, C. (2005) *Cell* **121,** 195–206
10. Wickner, R. B. (1994) *Science* **264,** 566–569
11. Peretz, D., Scott, M., Groth, D., Williamson, A., Burton, D., Cohen, F. E., and Prusiner, S. B. (2001) *Protein Sci.* **10,** 854–863
12. Peretz, D., Williamson, R. A., Legname, G., Matsunaga, Y., Vergara, J., Burton, D., DeArmond, S., Prusiner, S., and Scott, M. R. (2002) *Neuron* **34,** 921–932
13. Legname, G., Nguyen, H.-O. B., Baskakov, I. V., Cohen, F. E., DeArmond, S. J., and Prusiner, S. B. (2005) *Proc. Natl. Aca. Sci. U. S. A.* **102,** 2168–2173
14. Legname, G., Nguyen, H.-O. B., Peretz, D., Cohen, F. E., DeArmond, S. J., and Prusiner, S. B. (2006) *Proc. Acad. Natl. Sci. U. S. A.* **103,** 19105–19110
15. Baskakov, I. V., and Breydo, L. (2007) *Biochim. Biophys. Acta*, in press
16. Tanaka, M., Chien, P., Naber, N., Cooke, R., and Weissman, J. S. (2004) *Nature* **6980,** 323–328
17. Petkova, A. T., Leapman, R. D., Gua, Z., Yau, W.-M., Mattson, M. P., and Tycko, R. (2005) *Science* **307,** 262–265
18. Breydo, L., Bocharova, O. V., Makarava, N., Salnikov, V. V., Anderson, M., and Baskakov, I. V. (2005) *Biochemistry* **44,** 15534–15543
19. Bocharova, O. V., Breydo, L., Parfenov, A. S., Salnikov, V. V., and Baskakov, I. V. (2005) *J. Mol. Biol.* **346,** 645–659
20. Kaneko, K., Zulianello, L., Scott, M., Cooper, C. M., Wallace, A. C., James, T. L., Cohen, F. E., and Prusiner, S. B. (1997) *Proc. Natl. Acad. Sci. U. S. A.* **94,** 10069–10074
21. Prusiner, S. B., and Scott, M. R. (1997) *Annu. Rev. Genet.* **31,** 139–175
22. Bocharova, O. V., Breydo, L., Salnikov, V. V., Gill, A. C., and Baskakov, I. V. (2005) *Protein Sci.* **14,** 1222–1232
23. Krishnan, R., and Lindquist, S. (2005) *Nature* **435,** 765–772
24. Bocharova, O. V., Breydo, L., Salnikov, V. V., and Baskakov, I. V. (2005) *Biochemistry* **44,** 6776–6787
25. Anderson, M., Bocharova, O. V., Makarava, N., Breydo, L., Salnikov, V. V., and Baskakov, I. V. (2006) *J. Mol. Biol.* **358,** 580–596
26. Bocharova, O. V., Makarava, N., Breydo, L., Anderson, M., Salnikov, V. V., and Baskakov, I. V. (2006) *J. Biol. Chem.* **281,** 2373–2379
27. Prusiner, S. B., Bolton, D. C., Groth, D. F., Bowman, K. A., Cochran, S. P., and McKinley, M. P. (1982) *Biochemistry* **21,** 6942–6950
28. Flechsig, E., Shmerling, D., Hegyi, I., Raeber, A. J., Fischer, M., Cozzio, A., von Mering, C., Aguzzi, A., and Weissmann, C. (2000) *Neuron* **27,** 399–408
29. Wille, H., Michelitsch, M. D., Guenebaut, V., Supattapone, S., Serban, A., Cohen, F. E., Agard, D. A., and Prusiner, S. B. (2002) *Proc. Acad. Natl. Sci. U. S. A.* **99,** 3563–3568
30. Baskakov, I. V., and Bolen, D. W. (1998) *Biochemistry* **37,** 18010–18017
31. Santoro, M. M., and Bolen, D. W. (1988) *Biochemistry* **27,** 8063–8068
32. Ferreon, A. C., and Bolen, D. W. (2004) *Biochemistry* **43,** 13357–13369
33. O'Nuallain, B., Shivaprasad, S., Kheterpal, I., and Wetzel, R. (2005) *Biochemistry* **44,** 12709–12718
34. Williams, A. D., Shivaprasad, S., and Wetzel, R. (2006) *J. Mol. Biol.* **357,** 1283–1294
35. Narimoto, T., Sakurai, K., Okamoto, A., Chatani, E., Hoshino, M., Hasegawa, K., Naiki, H., and Goto, Y. (2004) *FEBS Lett.* **576,** 313–319
36. Baskakov, I. V., Legname, G., Gryczynski, Z., and Prusiner, S. B. (2004) *Protein Sci.* **13,** 586–595
37. Hosszu, L. L. P., Wells, M. A., Jackson, G. S., Jones, S., Batchelor, M., Clarke, A., Craven, C. J., Waltho, J. P., and Collinge, J. (2005) *Biochemistry* **44,** 16649–16657
38. Myers, J., Pace, C., and Scholtz, J. (1995) *Protein Sci.* **4,** 2138–2148
39. Schellman, J. A. (1978) *Biopolymers* **17,** 1305–1322
40. Carra, J. H., and Privalov, P. L. (1996) *FASEB J.* **10,** 67–74
41. Englander, S. W., Mayne, L., Bai, Y., and Sosnick, T. R. (1997) *Protein Sci.* **6,** 1101–1109
42. Novitskaya, V., Makarava, N., Bellon, A., Bocharova, O. V., Bronstein, I. B., Williamson, R. A., and Baskakov, I. V. (2006) *J. Biol. Chem.* **281,** 15536–15545
43. Baskakov, I. V., and Bocharova, O. V. (2005) *Biochemistry* **44,** 2339–2348
44. Moor, R. A., Herzog, C., Errett, J., Kocisko, D. A., Arnold, K. M., Hayes, S. F., and Priola, S. A. (2006) *Protein Sci.* **15,** 609–619
45. Leliveld, S. R., Dame, R. T., Wuite, G. J., Stitz, L., and Korth, C. (2006) *J. Biol. Chem.* **281,** 3268–3275
46. Dima, R. I., and Thirumalai, D. (2004) *Proc. Natl. Acad. Sci.* **101,** 15335–15340
47. Haire, L. F., Whyte, S. M., Vasisht, N., Gill, A. C., Verma, C., Dodson, E. J., Dodson, G. G., and Bayley, P. M. (2004) *J. Mol. Biol.* **336,** 1175–1183
48. Breydo, L., Sun, Y., Makarava, N., Lee, C.-I., Novitskaia, V., Bocharova, O. V., Kao, J. P. Y., and Baskakov, I. V. (2007) *Biochemistry* **46,** 852–861
49. Ziegler, J., Sticht, H., Marx, U. C., Muller, W., Rosch, P., and Schwarzinger, S. (2003) *J. Biol. Chem.* **278,** 50175–50181